Clean Techn Environ Policy (2016) 18:797–805
DOI 10.1007/s10098-015-1056-0

ORIGINAL PAPER

Effect of nitric acid modification on the lead(II) adsorption of mesoporous biochars with different mesopore size distributions

Kunquan Li[1] · Yuan Jiang[1] · Xiaohua Wang[1] · Di Bai[1] · Hua Li[1] · Zheng Zheng[2]

Received: 15 July 2015 / Accepted: 13 October 2015 / Published online: 24 October 2015

Abstract Two mesoporous biochars AC-1 and AC-2 with similar chemical properties but different mesopore size distributions were prepared to study the effect of HNO_3 modification on the lead(II) adsorption. AC-2 possesses higher mesopore volume and broader pore diameter than AC-1, while their surface area and micropore volume are similar. Adsorption experiments showed that AC-2 had far better removal efficiency, indicating the important role of mesopores played in the adsorption. HNO_3 modification enhanced the adsorption capacity of lead AC-1 and AC-2 by 15 and 27 mg g^{-1}, respectively. In particular, the removal rate of lead for AC-1 was improved from 46 to 99 % by HNO_3 treatment at a low initial lead concentration of 10 mg L^{-1}. Results of Boehm's titration demonstrated that the amounts of oxygenic acid groups of AC-1 and AC-2 increased to 2.456 and 2.705 mmol g^{-1} after HNO_3 treatment, respectively. Analyses of FTIR spectrum revealed that AC-2 was more likely to graft oxygen-containing acidic functional groups than AC-1, indicating that higher mesoporosity takes advantage of grafting more oxygenic functional groups, thus forming more active adsorption sites. The above results indicate that mesoporous biochars with wider pore width are more favorable to be introduced with oxygenic groups for enhanced lead removal efficiency.

Keywords Biomass carbon · Nitric acid modification · Adsorption · Adsorption isotherm

Introduction

Mesoporous carbons are gaining increased attention because of their excellent properties, such as high surface area, high pore volume, 3D structure, and high transfer speed. All these remarkable properties make mesoporous carbons suitable in removing organic chemicals and metal ions of environmental or economic concern from both potable and waste water (Gupta and Garg et al. 2015). In liquid-phase adsorption, the surface chemistry of solid adsorbents such as carbons, membranes, and resins plays a crucial role (Deng et al. 2015; Makkuni et al. 2005; Smuleac et al. 2005). For instance, the surface chemical properties of adsorbents have great effect on the adsorption interaction between adsorbent and polar or non-polar adsorbates (Lu et al. 2012; Bhattacharya et al. 1998, 2001; Ritchie et al. 1999). Increasing oxygen-containing acidic groups of an adsorbent can increase its electronegativity, resulting in a higher affinity and adsorption capacity for heavy metal ions (Liu et al. 2007; Cechinel et al. 2014).

Oxidation treatments are known to efficiently introduce oxygen-containing functional groups on carbons (Kyzas et al. 2013; Lu et al. 2012; Zhang et al. 2011). El-Hendawy (2003) proved that HNO_3 treatment promoted metal adsorption and pore diffusion of aqueous and hydrated lead ions with oxygen groups, enhancing the hydrophilic character of the carbon surface. Using HNO_3–NaOH surface modification, Liu et al. (2007) further showed that activated

Electronic supplementary material The online version of this article (doi:10.1007/s10098-015-1056-0) contains supplementary material, which is available to authorized users.

✉ Kunquan Li
kqlee@njau.edu.cn

[1] College of Engineering, Nanjing Agricultural University, Nanjing 210031, China

[2] Environmental Science & Engineering Department, Fudan University, Shanghai 200433, China

carbon containing more surface acidic groups has a higher Cr(VI) adsorption capacity than pristine carbon. In addition, Cechinel et al. (2014) carried out HNO_3 treatment on activated carbon of animal origin and found that chemical modification with HNO_3 increases the amount of acidic functional groups, in particular carboxylic groups, which are the facilitators of the adsorption and desorption processes. From these studies, subjecting carbon to HNO_3 treatment shows greater potential of removing heavy metal ions.

In general, depending on the ability of the oxidizing agent to diffuse inside the pores of activated carbon, the surface groups introduced appear to be located mainly inside the wide micropores and small mesopores, leading to blockage of the micropores and decreased adsorption efficiency (Ahmad et al. 2013; Mahurin et al. 2014). Mesoporous materials have not only large pore volume and wide pore size distribution but also unsaturated carbon atoms and structural defects which endow it with very strong reactivity. During modification, all these remarkable properties contribute to the fixation of a large amount of oxygen-containing acid functional groups on the carbon surface with partially narrowed pore dimensions which play a vital role in improving driving force and adsorption efficiency.

In this work, two highly mesoporous biochars with different mesopore size distributions were successfully prepared with phosphoric acid-microwave method and phosphoric acid low-temperature activation. The effect of HNO_3 treatment of mesoporous biochars with different mesopore size distributions on adsorption capacity was studied. The effect of initial lead ion concentration, solution pH, and the adsorption isotherms was also investigated to compare the adsorption characteristics and mechanism of Pb^{2+} on the different mesoporous biochars before and after modification.

Materials and methods

Reagents and instruments

Bagasse, phosphoric acid, nitric acid, lead nitrate, and other chemical reagents were of analytical grade and dissolved in deionized water. Main instruments include 3H-2000Ps2 surface area and pore size analyzer (Beishide Corporation, China), A3 flame atomic absorption spectrophotometer (Beijing Purkinje General Instrument Corporation), intelligent microwave carbon material preparation system (China Nanjing Yudian Automation Technology Co., Ltd), pipe furnace (Luoyang Bolaimaite Experiment Electric Furnace Co., Ltd), pH meter (Shanghai Kangyi Instrument Co., Ltd), and far-infrared laser spectrometer (NEXUS870 America-Nicolet).

Sample preparation and modification

Sample preparation

Bagasse was ground, dried, and sieved as received, and only particles with size less than 0.282 mm were selected for the preparation of activated carbon. The bagasse was then impregnated with phosphoric acid solution, resulting in H_3PO_4 acid/bagasse with a weight ratio (dry weight) of 1:1 for 24 h, and then dried in air at 105 °C for 10 h. After that, carbonization of acid-impregnated bagasse was carried out in a microwave activation device with activated power up to 900 W maintained for 22 min under inert nitrogen atmosphere (flow rate = 20 mL min^{-1}). After carbonization, the carbon was cooled to room temperature in a flow of nitrogen. To remove the phosphates, by-products of H_3PO_4 with bagasse, the obtained carbon after carbonization was firstly washed with 0.1 mol L^{-1} HCl for more than 12 h and then thoroughly washed with hot distilled water until the wash water attained a neutral pH. The sample was sifted through a 100-mesh sieve and marked as AC-1.

The dried, ground, and sifted bagasse was mixed with phosphoric acid solutions, resulting in H_3PO_4 acid/bagasse with an impregnated ratio (dry weight) of 1.5, and soaked for 24 h, then dried in air at 105 °C for 6 h. After that, carbonization was carried out in a pipe furnace by heating the acid-impregnated bagasse (5 °C min^{-1}) from room temperature to 500 °C (i.e., carbonization temperature) in a flow of nitrogen (20 mL min^{-1}) for 90 min. After carbonization, the carbon was cooled to room temperature in a flow of nitrogen. The product obtained was firstly smashed and screened through a mesh size of 100. To remove the phosphates, by-products of H_3PO_4 with bagasse, the sample was washed three times with 0.1 mol L^{-1} HCl for 12 h, followed by hot distilled water until the wash water attained a neutral pH. The sample was sifted through a 100-mesh sieve and marked as AC-2.

Modification of biochars

The modification was carried out by adding 150 mL of 32.5 % HNO_3 to 5 g of dried biochar placed in a conical glass flask. The mixture was heated at 60 °C under constant magnetic stirring for 5 h. The oxidized sample was sifted through a 100-mesh sieve and washed with hot distilled water until the wash water attained a neutral pH. The biochar samples prepared from AC-1 and AC-2 were identified to be AC-1–HNO_3 and AC-2–HNO_3, respectively.

Sample characterization

The pore structure characteristics of the samples were determined by nitrogen adsorption/desorption at 77 K

using a surface area analyzer, registered in the relative pressure (P/P_0) range of 10^{-3} to 0.99. Before analysis, samples were degassed under N_2 flow at 300 °C for 12 h. The surface area of the samples was estimated by BET method. The micropore volumes (V_{H-K}) and mesopore volumes (V_{BJH}) were calculated by applying Horvath–Kawazoe method and BJH method, respectively. DFT method was used to describe the pore size distribution of adsorbents. Total volume of pores was calculated from the single-point adsorption. The average pore size (D_p) was calculated from $4V_{total}/S_{total}$ by BET. SEM analysis (S-3400, Hitachi Corporation, Japan) was carried out to study surface texture and the development of porosity. The surface functional groups of the samples before and after adsorption were detected by FTIR spectrum and Boehm method. A Shimadzu XPS (AXIS-HS type) was employed to measure the element on the biochars' surface.

Adsorption experiment

Batch-mode adsorption studies were carried out using the necessary adsorbents in a 250-mL stopper conical flask containing 100 mL of test solution at a desired pH value, contact time, adsorbent dosage level, and solution temperature. A mass of 0.10 g of dried adsorbent was placed in contact with 100 mL of lead solution in concentrations ranging from 10 to 270 mg L^{-1} in an electrically thermostated reciprocating shaker at 25 °C with stirring at 150 rpm for 48 h to reach adsorption equilibrium conditions. According to kinetic experiments, it takes 4 h to attain equilibrium. The solution pH was adjusted to 4.5 during adsorption by adding 0.1 M HNO_3 and 0.1 M NaOH solution as required. The samples were then filtered, and the liquid phase was analyzed by A3 flame atomic absorption spectrophotometer. The removal rate (R, %) and adsorption amount of lead(II) per unit mass of adsorbent at equilibrium (q_e, mg g^{-1}) were calculated with the following equations:

$$q_e = V(C_0 - C_e)/m, \quad (1a)$$

$$R(\%) = (C_0 - C_e)/C_0 \times 100, \quad (1b)$$

where C_0 and C_e are the initial solution concentration and equilibrium concentration (mg L^{-1}), respectively, V is the volume of the solution, and m is the weight of biochar (g).

The effect of pH on the adsorption of lead(II) was carried out by equilibrating the adsorption mixture with 0.100 g dried adsorbent and 100 mL of 150 mg L^{-1} lead(II) solution at different pH from 2.0 to 8.0 at 25 °C. The optimum pH for the adsorption process was confirmed from the above experiment.

All the adsorption tests were carried out in triplicate to confirm reproducibility of the experimental results. The reproducibility and relative standard deviation (RSD) are less than 3 %.

Results and discussion

Characterization of samples

Pore characteristics of biochars

The nitrogen adsorption/desorption isotherms of the two biochars are shown in Fig. 1. As shown in Fig. 1a, in the low-pressure region where $P/P_0 < 0.2$, both nitrogen adsorption/desorption isotherms of AC-1 and AC-2 increased rapidly with increasing pressure, which is indicative of the presence of micropores (Li et al. 2014).

However, in the high-pressure region where P/P_0 is more than 0.4, the nitrogen adsorption of the two biochars showed different trends. AC-1 yields isotherms intermediate between type I and type II according to IUPAC (Lladó et al. 2015; Nabais et al. 2013). The nitrogen adsorption slowly increases with relative pressure (P/P_0) increasing to 0.4, suggesting that the reaction is a monolayer adsorption. In the high-pressure range where P/P_0 ranges from 0.4 to 0.7, a hysteresis loop was generated by the misalignment of the adsorption/desorption curves, which confirmed the occurrence of capillary condensation. The results show a noticeable development in mesopore

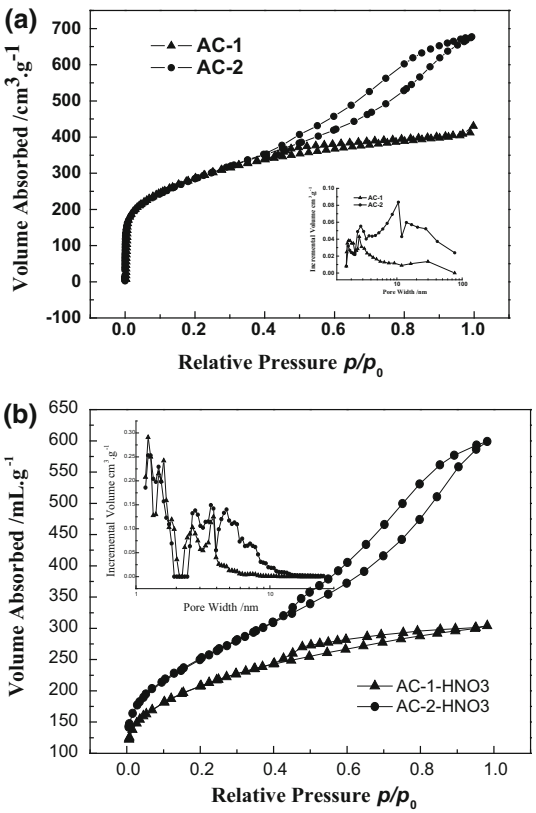

Fig. 1 N_2 adsorption/desorption isotherms of biochars before (**a**) and after (**b**) modification

Table 1 Physical and chemical properties of biochars

Samples	AC-1	AC-2	AC-1–HNO_3	AC-2–HNO_3
S_{BET} (m^2 g^{-1})	1021	1020	746	890
V_{total} (cm^3 g^{-1})	0.669	1.027	0.462	0.926
V_{H-K} (cm^3 g^{-1})	0.376	0.390	0.303	0.362
V_{BJH} (cm^3) g^{-1}	0.320	0.535	0.241	0.703
D_P (nm)	2.62	4.02	2.47	4.16
Carboxyl (mmol g^{-1})	0.5036	0.5097	1.5151	1.7144
Lactones (mmol g^{-1})	0.0454	0.1459	0.4265	0.4406
Phenolic (mmol g^{-1})	0.1037	0.2144	0.5146	0.5496

volume (Yeh et al. 2015). Table 1 summarizes the textural parameters of the original samples compared with those treated with nitric acid. The mesopore volume of AC-1 is 0.320 cm^3 g^{-1} (about 47.8 % of total volume).

The isotherm of AC-2 is type IV according to IUPAC nomenclature (Lladó et al. 2015), and an obvious hysteresis loop was generated, indicating abundance of mesopores. This isotherm type shows a quick increase in the adsorption of nitrogen because of capillary condensation, after which it plateaus, suggesting that adsorption occurred only on the external surface. According to the pore size distribution curve shown in Fig. 1a, AC-2 has a wider pore size distribution than AC-1. This assertion is corroborated from mesopore volumes summarized in Table 1.

As seen in Fig. 1b and Table 1, HNO_3 treatment leads to an appreciable loss of the micropore volumes (from 0.376 to 0.303 cm^3 g^{-1} and from 0.390 to 0.362 cm^3 g^{-1}, respectively) and a small increase in mesoporosity (from 47.6 to 52.2 % and from 52.1 to 75.9 %, respectively), probably by blocking partial micropores and oxidizing deposited carbon that blocks pore opening, thus creating some mesoporosity. These results must be linked to the adsorption properties of the biochars, and this possible dependence is investigated in the "Effect of nitric acid modification on the adsorption" section.

SEM analysis of samples

In Fig. 2 are shown the scanning electron microscope images of the two prepared biochars. SEM micrographs show that the two prepared biochars have well-developed micropores and mesopores with network nanostructure (Jia et al. 2014). Comparing Fig. 2a, b, AC-2 has more mesopores than AC-1.

Adsorption studies

Effect of mesopore distribution

The adsorption capacities for Pb^{2+} of the two pristine biochars with different mesopore structures are shown in Fig. S1. The adsorption experiments were performed as follows: 0.10 g biochar was added into 100 mL Pb(II) solution at pH 4.5 in a reciprocating shaker at 25 °C with stirring at 150 rpm for 48 h to reach adsorption equilibrium conditions.

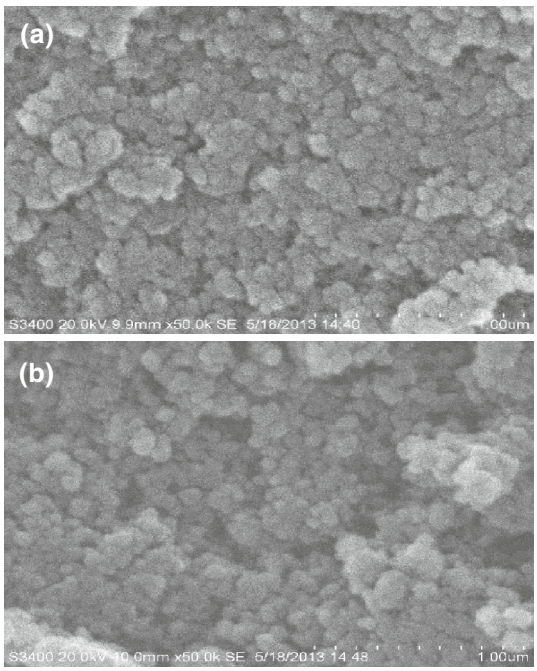

Fig. 2 SEM images of the two biochars AC-1 (**a**) and AC-2 (**b**)

As shown in Fig. S1, the saturation amount of Pb^{2+} adsorbed by AC-1 is higher than that by AC-2. The difference of removal efficiency of lead for the two biomass chars should be due to their different mesopore structures. As shown in Table 1, although the two biochars AC-1 and AC-2 have the similar surface area, chemical groups and micropore volume, the mesopore volume of AC-2 is 67 % higher than that of AC-1. In the adsorption process of lead onto carbon, mesopores may play a considerable role not only in accelerating the diffusion of lead into micropores, but also in increasing the lead equilibrium coverage of the micropore surface, which results in the higher adsorption capacity of lead on the carbon with larger mesopore.

It is generally believed that the micropore of activated carbon is the major provider of adsorptive sites in aqueous solutions, whereas the adsorption in mesopore is weaker. Thus, the adsorption on activated carbon would undergo a series of steps of lead diffusion from the bulk phase into mesopores and then to micropores. One study has shown that the surface of the micropores might not be completely occupied in adsorption, and the fractional coverage of micropore surface depends on the length of the diffusion path (Teng and Hsieh 1998). In the process of adsorbate diffusion in micropores, pore blockage may occur due to the cross-sectional area of some throats in micropores for adsorbate to penetrate (McKay 1985). Therefore, a longer diffusion path of micropore will lead to a greater probability for the pore blockage to occur and, thus, a smaller coverage.

With the presence of mesopores in carbon, the path length of micropores for the diffusion from mesopores to the carbon interior will be shorter than that when the diffusion comes directly from the bulk phase to the interior without the aid of mesopores. Hence, the higher lead capacities of AC-2, which has a similar micropore volume with AC-1 but higher mesoporosity, can thus be explained by the fact that the higher mesopore volume of AC-2 shortened the access of lead ions to the interior micropores and thus increased the lead equilibrium coverage of the micropore surface.

Effect of nitric acid modification

The effect of nitric acid modification on Pb^{2+} uptake from aqueous solutions is presented in Fig. 3. HNO_3 treatment of biochars promotes Pb^{2+} uptake, with adsorption capacity increasing by 15 and 27 mg g^{-1} for AC-1 and AC-2, respectively (i.e., a mean adsorption value of 99 mg g^{-1} as compared to the value for non-modified AC-1 of 84 mg g^{-1}, as well as a mean value of 118 mg g^{-1} as compared to the value for non-modified AC-2 of 91 mg g^{-1}). The adsorption mechanism of heavy metal ions includes three aspects (Xu et al. 2010): (a) physical adsorption resulting from heavy metal ions depositing on the carbon surface; (b) ion exchange reaction occurring on the surface; and (c) chemical adsorption caused by the reaction between heavy metal ions and oxygen-containing functional groups.

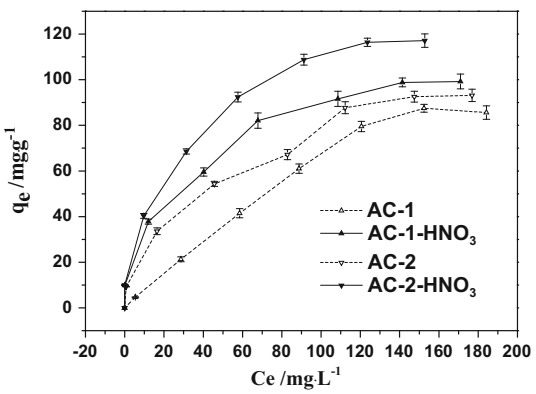

Fig. 3 The effect of nitric acid modification on Pb^{2+} uptake at 25 °C

Two reasons may explain the higher adsorption capacity of Pb^{2+} of AC-1–HNO_3 and AC-2–HNO_3 than the pristine biochars AC-1 and AC-2. On the one hand, HNO_3 treatment of biochars probably resulted in dissolution of some permeated inorganic matter and oxidation of deposited carbon that blocks pore opening, thus creating some mesopores. On the other hand, nitric acid modification increases the amount of oxygen-containing acidic functional groups, such as carboxyl groups, carbonyl groups, phenolic hydroxyl groups, and lactone groups. As a result, pH_{PZC} decreased, and modified biochars, with relatively high acidity, show a higher affinity for lead ions. Metal ion uptake has been demonstrated to be a polar or acidic function resulting from electrostatic attraction of metal ions to oxygen-containing functional groups (Deng et al. 2015; Eldridge et al. 2015; Sun et al. 2011; Ahmad et al. 2013).

The data in Table 1 demonstrate that HNO_3 treatment of biochars leads to a considerable loss in the total surface area of 26.9 and 12.7 % and the micropore volume of 19.4 and 7.2 %, as well as an increase in the mesopore proportion of 52.2 and 75.9 % for AC-1–HNO_3 and AC-2–HNO_3, respectively. Compared with non-modified samples, mesopore volume of AC-2–HNO_3 improved, whereas that of AC-1–HNO_3 decreased, which can be attributed to two factors: AC-2 has a wider pore size distribution, and thus macropores shrunk to form mesopores after grafting oxygen-containing acid functional groups; pore size distribution of pristine AC-1 mainly ranges from 2 to 5 nm, with some mesopores blocked during modification resulting in reduced mesopore volume.

Figure 3 shows that the adsorption capacity of AC-2–HNO_3 for lead ions outperformed AC-1–HNO_3, highlighting the importance of mesopores in pristine biochars. During HNO_3 treatment, oxygen-containing acidic functional groups are easier to be grafted onto AC-2 because of its higher mesoporosity. The oxidized biochar AC-1–HNO_3 has smaller micropore volume and mesopore volume than AC-1 and AC-2. However, it has the highest adsorption capacity among the three biochars, proving that pore structure is not the only determining factor in influencing Pb^{2+} uptake, which in turn emphasizes the vital function of surface chemical functional groups on the surface of adsorbent.

Figure 4 shows the FTIR spectra of AC-1 and AC-2, as well as their HNO_3-oxidized forms. The adsorption bands observed demonstrate that HNO_3 treatment efficiently

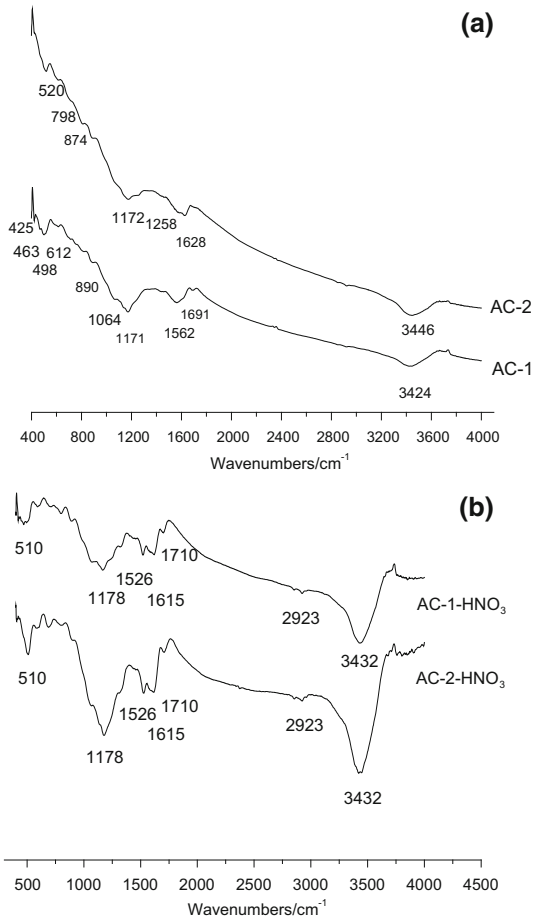

Fig. 4 FTIR spectra of biochars *before* (**a**) and *after* modification (**b**)

increases the amounts of oxygen-containing functional groups. The shoulders observed at 510, 1175, 1526, 1625, 1710, 2923, and 3436 cm^{-1} on AC-1 and AC-2 are often ascribed to hydrocarbon out-of-plane bending, as well as stretching vibrations of ether, ketone, aldehyde, and hydrogen groups. Furthermore, spectrum vibration of AC-2–HNO_3 was more intense than that of AC-1–HNO_3, suggesting that AC-2–HNO_3 has more abundant acidic functional groups than AC-1–HNO_3. This is further confirmed by Boehm's titration. In addition, according to the results of the XPS, the percentages of P in AC-1, AC-2, AC-1–HNO_3, and AC-2–HNO_3 are 4.63, 4.59, 0.63, and 0.47 %, respectively. Hence, those small shoulders at 500–800 and 1070–1090 cm^{-1} could also be ascribed to P–C phosphorus-containing compounds and ionized linkage P^{+}–O^{-} in acid phosphates, respectively (Liu et al. 2012; Wang 2011), which can effectively bind Pb(II) to the surface by generating strong chemisorption bonds or ion exchange as similar as oxygen-containing functional groups do (Huang 2014).

The results of Boehm's titration of the biochars before and after HNO_3 are presented in Table 1. Table 1 shows that the amounts of oxygenic acid groups of AC-1 and AC-2 increased about 1.5–4.0 times after HNO_3 treatment. From AC-1 to AC-1–HNO_3, the amount of carboxyl and lactone groups and phenolic hydroxyl increased from 0.5036 to 1.5151 mmol g^{-1}, from 0.0454 to 0.4265 mmol g^{-1}, and from 0.1037 to 0.5146 mmol g^{-1}, and from AC-2 to AC-2–HNO_3, the amount of carboxyl and lactone groups and phenolic hydroxyl increased from 0.5097 to 1.7144 mmol g^{-1}, from 0.1459 to 0.4406 mmol g^{-1}, and from 0.2144 to 0.5496 mmol g^{-1}, respectively. AC-2–HNO_3 has more oxygenic acidic functional groups than AC-1–HNO_3, which is in accordance with FTIR spectrum analysis. This phenomenon further indicates that mesopore structure plays a vital important role in the introduction of acidic functional groups via HNO_3 treatment, and the increased amount of oxygen-containing functional groups explains the improved adsorption capacity of HNO_3-modified biochars. Meanwhile, higher mesopore volume and wider pore width take advantage of grafting more oxygenic acidic functional groups.

Effect of initial lead ion concentration

As seen in Fig. S2, although AC-1 exhibits superior adsorption, it still cannot effectively remove lead ions even in low initial concentrations, thus affecting its utility. In contrast, AC-2, AC-1–HNO_3, and AC-2–HNO_3 exhibited increased Pb^{2+} removal rate with decreased concentration, suggesting favorable adsorption. Moreover, in the case of oxidized biochars AC-1–HNO_3 and AC-2–HNO_3, Pb^{2+} uptake is considerably higher in comparison to that of non-oxidized biochars. Moreover, as initial concentration of lead Pb^{2+} is less than 10 mg L^{-1}, the removal rates of Pb^{2+} by the two oxidized biochars are $\sim$100 %. These results show that HNO_3 treatment efficiently enhances the binding energy, forcing active sites to capture lead ions. AC-2–HNO_3 has a higher Pb^{2+} adsorption capacity than AC-1–HNO_3 regardless of the initial concentration because the former has more effective active sites resulting in more mesopore volume and oxygen-containing acidic functional groups formed from HNO_3 treatment.

Effect of solution pH

Since the surface charge of an adsorbent can be modified by changing the pH of the solution, pH is one of the most important parameters influencing the adsorption process of metal ions. As a function of solution pH, Pb^{2+} is the dominant species below a pH value of about 6. Between pH 6.0 and 8.0, lead undergoes hydrolysis to $Pb(OH)^{+}$. Above

pH 9.0, solid lead hydroxide $Pb(OH)_2$ is thermodynamically the most stable phase, while $Pb(OH)_3^-$ is predominant at pH above 11. The pH was set between 2.0 and 8.0 to prevent precipitation of metals in the form of hydroxides under alkaline pH.

As described in the previous section, the surfaces of the HNO_3-oxidized mesoporous biochars mainly display AC–COOH, AC–OH, and AC–O–$OPO(OH)_2$ functional groups. Thus adsorption reaction, for Pb(II), can be described by the following expressions:

$$R_{AC}-COOH + Pb^{2+} \rightarrow R_{AC}-COOPb^{+} + H^{+} \quad (2a)$$

$$R_{AC}-OH + Pb^{2+} \rightarrow R_{AC}-COPb^{+} + H^{+} \quad (2b)$$

$$R_{AC}-COOH + PbOH^{+} \rightarrow R_{AC}-COOPb(OH) + H^{+} \quad (2c)$$

$$R_{AC}-OH + Pb(OH)^{+} \rightarrow R_{AC}-COPb(OH) + H^{+} \quad (2d)$$

$$R_{AC}-COPO(OH)_2 + 2Pb^{2+} \rightarrow R_{AC}-COPOOPb_2^{2+} + 2H^{+}, \quad (2e)$$

where R_{AC} denotes the biochar surface. The surface functional groups may exchange a proton with positively charged Pb(II) species in aqueous solution forming ion-exchanged complex.

Figure 5 clearly shows a sharp increase in the adsorption amount of Pb^{2+} by the four mesoporous biochars up to pH 4.0, followed by a slight increase to an approximate constant at pH 4.5–6.5 for the oxidized biochars and at pH 5.5–6.5 for the pristine biochars. At low pH range below pHzpc between 2.0 and 4.0, hydrogen ions compete with Pb^{2+} for the surface of the biochars which would hinder Pb(II) ions from reaching the binding sites of the sorbent caused by the repulsive forces. As pH is above pHzpc, the surface of adsorbent shows negative and strong electrostatic attraction between surface groups and Pb(II) species, favoring the Pb(II) adsorption. The modification of nitric acid oxidation decreases the pHzpc of biochars. Thus, the optimum pH values of lead adsorption for the two oxidized biochars are lower than the corresponding pristine biochars.

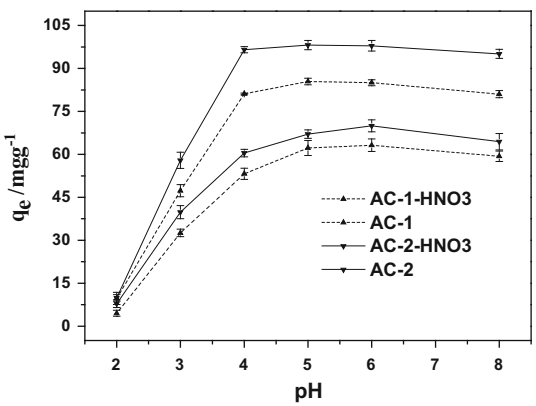

Fig. 5 Effect of solution pH on Pb^{2+} removal at 25 °C

Adsorption isotherms

The experimental data were used to fit Langmuir, Freundlich, Redlich–Peterson, and Temkin isotherm models to better understand the adsorption mechanism. The widely used Langmuir isotherm model suggests that the surface of the adsorbent is uniform and no interactions between adsorbate molecules on adjacent sites exist (Thilagavathy and Santhi 2014). Both Freundlich and Temkin isotherms assume that lead ion uptake occurs on a heterogeneous surface by multilayer adsorption (Ucar et al. 2014). However, derivation of Temkin isotherm assumes that because of adsorbate/adsorbent interactions, the heat of adsorption decreases linearly rather than logarithmically, as implied in the Freundlich equation (Shrestha et al. 2013; Pourreza et al. 2015). Redlich–Peterson isotherm is a combination of Langmuir and Freundlich with three parameters (El Nemr et al. 2015). Parameter n in the Freundlich model reflects the heterogeneity of the adsorbent and the intensity of adsorption. A higher value of n is better, with a value between 2 and 10 generally considered as easily adsorbed (Shrestha et al. 2013; Xu et al. 2013).

As listed in Table 2, the determination coefficient (R^2) of Langmuir was higher than 0.97, but the maximum saturated monolayer adsorption capacity q_{cac}^0 was found to be far more than the experimental data q_{exp}^0 suggesting that Langmuir isotherm does not fit well to the experimental data. The adsorption of lead ions onto biochar surfaces is non-uniform (Xu et al. 2010). The Freundlich model best described Pb^{2+} adsorption onto biochars as R^2 values are greater than 0.97, indicating that Freundlich can well describe the adsorption. The Freundlich constant n for AC-1 is less than 2, indicating that the adsorption of lead on AC-1 was unfavorable. The n values for AC-2, AC-2–HNO_3, and AC-1–HNO_3 are higher than 2, indicating that these adsorption reactions are favorable and can be characterized by a concave Freundlich isotherm, suggesting that significant adsorption takes place at low concentrations, but the increase in the amount adsorbed with concentration becomes less significant at higher concentrations. Furthermore, the order of K_F values before and after modification is as follows: $KF_{AC\text{-}2\text{–}HNO3} > KF_{AC\text{-}2}$ and $KF_{AC\text{-}1\text{–}HNO3} > KF_{AC\text{-}1}$, which supports the conclusion that adsorption capacity can be improved via HNO_3 treatment. Freundlich correlation coefficient (R^2) was found to be better than that of Temkin, indicating that the heat of adsorption decreased logarithmically with increase in adsorption capacity.

Table 2 Isotherm parameters for lead(II) adsorption by biochars before and after modification

Isotherm models	Parameters	AC-1	AC-1–HNO_3	AC-2	AC-2–HNO_3
Langmuir $q_e = bq^0c_e\ (1 + bc_e)$	$q^0_{exp}\ (mg\ g^{-1})$	84	99	91	118
	$q^0_{cac}\ (mg\ g^{-1})$	182	118	123	141
	b/L mg^{-1}	0.006	0.031	0.018	0.034
	R^2	0.984	0.982	0.979	0.988
Freundlich $q_e = K_Fc_e^{1/n}$	K_F (L $mg^{-1)}$	2.670	10.39	17.59	20.61
	n	1.460	2.307	2.893	2.804
	R^2	0.970	0.989	0.989	0.987
Redlich–Peterson $q_e = K_Rc_e\ (1 + ac_e^{ß})$	K_R (L $mg^{-1)}$	0.7227	726,547	155	6.439
	a (L $mg^{-1)}$	1.169E−9	41,299	14.49	0.085
	$ß$	3.828	0.6543	0.572	0.880
	R^2	0.999	0.986	0.986	0.988
Temkin $y = BlnA_T + Blnx$	A_T (L $mg^{-1)}$	0.1446	14.02	1.351	31.042
	B (L $mg^{-1)}$	25.25	11.66	15.787	12.418
	R^2	0.916	0.895	0.917	0.886

Conclusion

Two biochars with approximately similar surface areas but different pore structures were prepared from bagasse by phosphoric acid-microwave method and phosphoric acid low-temperature activation. Results from adsorption experiments show that AC-2 with larger mesopore volume and wider pore size distribution shows a higher adsorption capacity and removal rate of Pb^{2+} than AC-1, especially at initial lead concentration below 50 mg L^{-1}, indicating that increasing the mesoporosity can help capturing Pb^{2+} from dilute solution. Liquid-phase oxidation of biochars derived from bagasse using HNO_3 results in considerable modification of their surface chemistry and adsorption properties. The Boehm's titration results demonstrated that the amounts of oxygenic acid groups of AC-1 and AC-2 increased about 1.5–4.0 times after the HNO_3 treatment. FTIR spectra and Boehm's titration suggest that AC-2–HNO_3 has more abundant oxygen-containing acidic functional groups than AC-1–HNO_3 because of its higher mesopore volume and wider mesopore size, emphasizing that mesopore structure plays a vital role in grafting oxygen-containing acidic functional groups during nitric acid modification. Liquid-phase oxidation with HNO_3 promotes an increase in lead ion removal rate as a result of abundantly generated oxygen-containing functional groups. Moreover, mesopore volume of AC-2–HNO_3 was enhanced from 0.535 to 0.703 $cm^3\ g^{-1}$, whereas AC-1–HNO_3 showed a decreased mesoporosity. The results indicate that a lager mesopore volume and size take advantage of the introduction of more oxygenic functional groups, as well as mesopore volume, thus improving the adsorption ability and efficiency. The Freundlich isotherm model best fits the experimental data, illustrating that the main adsorption site is the non-uniform pore or surface, indicating that the heat of adsorption decreased logarithmically with an increase in adsorption capacity. The results of the present study indicate that mesoporous biochars with wider pore width are more favorable to be introduced with oxygenic groups and mesopores for enhanced lead removal efficiency.

Acknowledgments The authors gratefully acknowledge the research grant provided by the Natural Science Foundation of China (No. 51102136), the Doctoral fund of Ministry of Education of China (No. 20110097120021), and China's Postdoctoral Science Fund (No. 2014M560429).

References

Ahmad F, Daud WMAW, Ahmad MA, Radzi R (2013) The effects of acid leaching on porosity and surface functional groups of cocoa (*Theobroma cacao*)-shell based activated carbon. Chem Eng Res Des 91(6):1028–1038

Bhattacharya DB, Bachas LG, Hestekin J, Richie S, Sikdar SK (1998) Novel polyglutamic acid functionalized microfiltration membranes for sorption of heavy metals at high capacity. J Membr Sci 141:121–135

Bhattacharya DB, Bachas LG, Ritchie S, Sikdar SK (2001) Polycysteine functionalized microfiltration membranes for heavy metal capture. EST 35:3252–3258

Cechinel MAP, Ulson de Souz SMAG, Ulson de Souza AA (2014) Study of lead(II) adsorption onto activated carbon originating from cow bone. J Clean Prod 65:342–349

Deng S, Zhang G, Wang X, Zheng T, Wang P (2015) Preparation and performance of polyacrylonitrile fiber functionalized with iminodiacetic acid under microwave irradiation for adsorption of Cu(II) and Hg(II). Chem Eng J 276:349–357

El Nemr A, El Sikaily A, Khaled A, Abdelwahab O (2015) Removal of toxic chromium from aqueous solution, wastewater and saline

water by marine red alga *Pterocladia capillacea* and its activated carbon. Arab J Chem 8(1):105–117

Eldridge DS, Crawford RJ, Harding IH (2015) The role of metal ion-ligand interactions during divalent metal ion adsorption. J Colloid Interface Sci 454:20–26

El-Hendawy ANA (2003) Influence of HNO_3 oxidation on the structure and adsorptive properties of corncob-based activated carbon. Carbon 41:713–722

Gupta A, Garg A (2015) Primary sewage sludge-derived activated carbon: characterisation and application in wastewater treatment. Clean Technol Environ 17(6):1619–1631

Huang Y, Li S, Chen J, Zhang X, Chen Y (2014) Adsorption of Pb(II) on mesoporous activated carbons fabricated from water hyacinth using H_3PO_4 activation: adsorption capacity, kinetic and isotherm studies. Appl Surf Sci 293:160–168

Jia JQ, Li KQ, Zhang YX, Qiao XD (2014) Adsorption characteristics of methylene blue onto biomass-based porous activated carbons by microwave assisted H_3PO_4 activation. Chin J Environ Eng 8(1):92–97 **(in Chinese)**

Kyzas GZ, Lazaridis NK, Deliyanni EA (2013) Oxidation time effect of activated carbon for drug adsorption. Chem Eng J 234:491–499

Li K, Yang M, Wang J (2014) Preparation of amine-modified mesoporous activated carbon and its adsorption of lead(II) from aqueous solution. Chin Environ Sci 34(8):1985–1992 **(in Chinese)**

Liu S, Chen X, Chen X, Liu Z, Wang H (2007) Activated carbon with excellent chromium (VI) adsorption performance prepared by acid-base surface modification. J Hazard Mater 141:315–319

Liu H, Zhang J, Bao N, Cheng C, Ren L (2012) Textural properties and surface chemistry of lotus stalk-derived activated carbons prepared using different phosphorus oxyacids: adsorption of trimethoprim. J Hazard Mater 235–236:367–375

Lladó J, Lao-Luque C, Ruiz B, Fuente E, Solé-Sardans M, Dorado AD (2015) Role of activated carbon properties in atrazine and paracetamol adsorption equilibrium and kinetics. Process Saf Environ 95:51–59

Lu X, Jiang J, Sun K, Xie X, Hu Y (2012) Surface modification, characterization and adsorptive properties of a coconut activated carbon. Appl Surf Sci 258(20):8247–8252

Mahurin SM, Gorka J, Nelson KM, Mayes RT, Dai S (2014) Enhanced CO_2/N_2 selectivity in amidoxime-modified porous carbon. Carbon 67:457–464

Makkuni A, Bachas LG, Bhattacharya D, Varma RS, Sikdar SK (2005) Aqueous and vapor phase mercury sorption by inorganic oxide materials functionalized with thiols and polythiols. Clean Tsechnol Environ Policy 7:87–96

McKay G, Bino MJ, Altamemi AR (1985) The adsorption of various pollutants from aqueous solutions on to activated carbon. Water Res 19:91–495

Nabais JMV, Laginhas C, Carrott MMLR, Carrott PJM, Amorós JEC, Gisbert AVN (2013) Surface and porous characterisation of activated carbons made from a novel biomass precursor, the esparto grass. Appl Surf Sci 265:919–924

Pourreza N, Rastegarzadeh S, Larki A (2015) Nano-TiO_2 modified with 2-mercaptobenzimidazole as an efficient adsorbent for removal of Ag(I) from aqueous solutions. J Ind Eng Chem 20(1):127–132

Ritchie SMC, Bachas LG, Olin T, Sikdar SK, Bhatacharya DB (1999) Surface modification of silica- and cellulose-based microfiltration membranes with functionalized polyamino acids for heavy metal sorption. Langmuir 15(19):6346–6357

Shrestha S, Son G, Lee SH, Lee TG (2013) Isotherm and thermodynamic studies of Zn(II) adsorption on lignite and coconut shell-based activated carbon fiber. Chemosphere 92:1053–1061

Smuleac V, Butterfield DA, Sikdar SK, Varma RS, Bhattacharya D (2005) Polythiol-functionalized alumina membranes for mercury capture. J Membr Sci 251:169–178

Sun X, Hwang JY, Xie S (2011) Density functional study of elemental mercury adsorption on surfactants. Fuel 90(3):1061–1068

Teng H, Hsieh CT (1998) Influence of surface characteristics on liquid-phase adsorption of phenol by activated carbons prepared from bituminous coal. Ind Eng Chem Res 37:3618–3624

Thilagavathy P, Santhi T (2014) Kinetics, isotherms and equilibrium study of Co(II) adsorption from single and binary aqueous solutions by *Acacia nilotica* leaf carbon. Chin J Chem Eng 22:1193–1198

Ucar S, Erdem M, Tay T, Karagoz S (2014) Removal of lead(II) and nickel(II) ions from aqueous solution using activated carbon prepared from rapeseed oil cake by Na_2CO_3 activation. Clean Technol Environ 17:747–756

Wang Z, Nie E, Li J, Zhao Y, Luo X, Zheng Z (2011) Carbons prepared from *Spartina alterniflora* and its anaerobically digested residue by H_3PO_4 activation: characterization and adsorption of cadmium from aqueous solutions. J Hazard Mater 188(1–3):29–36

Xu X, Liu B, Deng Z (2010) Analysis of decisive parameters in activated carbon's adsorption of heavy metals. Energy Environ 24(2):48–50 **(in Chinese)**

Xu C, Liu F, Chao L, Zhu C, Li A (2013) Synthesis of polyamine chelating resins and adsorption properties toward heavy metal ions from aqueous media. Ion Exch Adsorpt 29(6):481–495 **(in Chinese)**

Yeh CL, Hsi HC, Li KC, Hou CH (2015) Improved performance in capacitive deionization of activated carbon electrodes with a tunable mesopore and micropore ratio. Desalination 367:60–68

Zhang X, Deng S, Liu Q, Zhang Y, Cheng L (2011) Surface functional groups and redox property of modified activated carbons. Min Sci Techol 21(2):181–184